Available online at www.sciencedirect.com
ScienceDirect
Journal of the European Ceramic Society 28 (2008) 499–504
www.elsevier.com/locate/jeurceramsoc

The electronic properties of complex oxides of bismuth with the mullite structure

Kenneth J.D. MacKenzie *, Troy Dougherty, Jeremie Barrel

MacDiarmid Institute for Advanced Materials and Nanotechnology, School of Chemical and Physical Sciences, Victoria University of Wellington, New Zealand

Available online 6 April 2007

Abstract

Bismuth forms double oxides with the oxides of aluminium, gallium, iron and manganese, all of which have the mullite structure. Since other bismuth-based complex oxides show useful functional properties including high-temperature pyroelectricity and piezoelectricity, the electronic and magnetic properties of the mullite-structured bismuth compounds are of potential interest.

In the present study, all the above compounds were synthesised in pure form by solid-state reaction, and their thermal behaviour and structures characterised by thermal analysis, powder X-ray diffraction, solid-state MAS NMR and Mőssbauer spectroscopy as appropriate.

The thermal analysis information allowed highly sintered polycrystalline samples to be produced. After the application of silver electrodes, the electronic properties of the pellet samples were determined as a function of frequency and temperature up to 900 °C. Frequency-dependent inflexions in the relative permittivity and loss angle curves of the ferrate and gallate may be due to losses due to dielectric relaxation, but the most notable and consistent electronic phenomenon in all samples is a steep rise in the dc conductivity at higher temperatures. The *P–E* hysteresis loops for the ferrate and manganate indicate that these are very poor ferroelectric materials, consistent with the centrosymmetric crystal structure of all these compounds.

Keywords: Bismuth compounds; Powders-solid state reaction; Spectroscopy; X-ray methods; Electrical properties

1. Introduction

In the last decade, ceramic materials previously considered interesting for their mechanical or engineering properties have increasingly been reinvestigated for other potentially useful functional properties, especially their electronic properties. The aluminosilicate mullite is an example of a material with excellent thermal and mechanical properties at elevated temperatures, making is an important engineering material.[1] Pure mullite is an insulator, allowing it to be used as a substrate for electronic devices,[1] but doping with transition metals is reported[2] to lower the resistivity by two orders of magnitude, to about 10^{11} Ω cm at room temperature.

The dielectric properties of aluminosilicate mullite, which are also important in determining its usefulness as an electronic substrate material, have also been determined.[3,4] The spread in the reported dielectric constants of 6.7–7.5 at 1 MHz has been ascribed to differences in chemical composition and microstructure of the ceramic samples, and in the proportion of glassy intergranular phases.[3] The dielectric constants remain more or less constant over a wide frequency range, up to 14 GHz.[4] These data, and the low dielectric loss of pure mullite confirm its useful high-frequency insulating properties.

These conclusions are not unexpected, but indicate that materials with the mullite structure which may also display useful electronic functions should be sought in systems containing other elements. One such group of mullite-structured compounds based on bismuth oxide (bismuth aluminate, ferrate, gallate and manganate) was first reported by Levin and Roth[5] without supporting X-ray structural data. The mullite-related structures of the aluminate and ferrate compounds were determined by single-crystal X-ray studies in the same year by Koizumi and Ikeda,[6] with X-ray determinations of the manganate[7] and gallate[8] following in 1967 and 1971, respectively. Subsequent refinements of these crystal structures[9–12] indicate that they all have orthorhombic unit cells in the space group *Pbam* with $z = 2$. The unit cell parameters are shown in Table 1, together with mullite for comparison.

* Corresponding author. Fax: +64 4463 5237.
E-mail address: kenneth.mackenzie@vuw.ac.nz (K.J.D. MacKenzie).

0955-2219/$ – see front matter © 2007 Elsevier Ltd. All rights reserved.
doi:10.1016/j.jeurceramsoc.2007.03.012

Table 1
X-ray structural data for bismuth aluminate, ferrate, gallate and manganate, with mullite, for comparison

	$Bi_2Al_4O_9$	$Bi_2Fe_4O_9$	$Bi_2Ga_4O_9$	$Bi_2Mn_4O_{10}$	Mullite
Space group	*Pbam*	*Pbam*	*Pbam*	*Pbam*	*Pbam*
$a \pm 0.005$	7.712	7.950	7.934	7.540	7.545
$b \pm 0.005$	8.112	8.428	8.301	8.534	7.689
$c \pm 0.005$	5.708	6.005	5.903	5.766	2.884
Z	2	2	2	2	1

Cell parameters taken from reference[12], mullite parameters from reference[1].

In the structures of the Al, Fe and Ga compounds all these atoms are distributed evenly across the tetrahedral M1 and octahedral M2 sites. By contrast, in the structure of the Mn compound, which has the formula $Bi_2Mn_4O_{10}$,[12] the Mn atoms are evenly distributed over the tetrahedral M2 and square pyramidal M3 sites. The Bi M4 atoms are three-coordinated, with three more oxygens in the outer sphere.[12] A view of the bismuth aluminate structure, looking down the octahedral chains, is shown in Fig. 1, together with the same view of mullite, for comparison.

Table 1 shows that the by comparison with mullite, the Bi double oxides have two formula units in the unit cell, resulting in the doubling of their *c*-axis dimensions. In the *c*-axis direction, an identical unit cell in mullite would be rotated by 180° in the Bi-compounds. The structural features common to the Bi-compounds and mullite are the columns of octahedral chains cross-linked by tetrahedral units (Fig. 1).

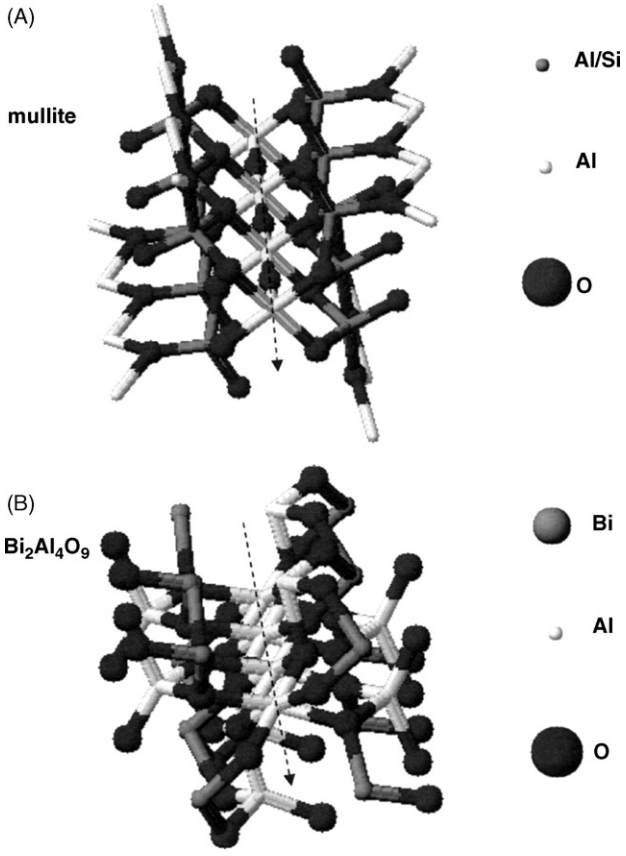

Fig. 1. View down the octahedral columns of (A) mullite and (B) $Bi_2Al_4O_9$, showing the tetrahedral cross-linking chains. Diagram prepared using ACD Chemsketch 3D software.

Although Bi compounds in general often display interesting electronic properties, not a great deal of work has been reported on the properties of these mullite-structured materials. The electric conductivity of the aluminate, reported to be 10^{-2} S cm^{-1} at 800 °C[13] was suggested to be largely, but not completely, ionic. A more detailed mechanism has been proposed for oxide ion conductance in this compound, invoking the polarizability of the Bi 6 s^2 lone pairs of electrons.[14]

Although the magnetic properties of the ferrate have been more extensively investigated,[15–23] suggesting the occurrence of a paramagnetic-to-antiferomagnetic transition at a Neel temperature of −9 °C the electronic properties of this and the other isostructural compounds have not been investigated systematically. The present study aims to remedy this deficiency by investigating the electronic behaviour of a series of well-characterized sintered polycrystalline samples as a function of temperature and frequency. Although all the structures as represented in Table 1 and Fig. 1 are centro-symmetric and would not therefore be expected to show ferroelectric properties, the possibility that small variations in the structure, stoichiometry or grain-boundary phases may contribute to electronic effects was thought to justify the present study.

2. Experimental

The starting materials were Bi_2O_3, 99.9 mass%, −325 mesh (Cerac Specialty Inorganics), calcined Al_2O_3, 99.5 mass% (AnalaR), Fe_2O_3, 99.5% (Alfa), Ga_2O_3, 99.99 mass% (Aldrich) and Mn_2O_3, 99 mass%, −325 mesh (Aldrich). The double oxides were synthesised by solid-state reaction between 1:2 mixtures of the reactant powders. Before firing, the mixtures were homogenised by ball-milling in 2-propanol for 12 h. After removal of the solvent by rotary evaporation at 105 °C, the powders were formed into pellets by uniaxially pressing at 10 MPa, or by CIPing at 250 MPa. Firing and sintering was carried out in static air in an Amalgams CH5 chamber furnace at temperatures determined on the basis of TGA/DSC measurements (Rheometrics STA 1500 thermal analyser, heating rate 10 °C min^{-1}, in flowing air, 50 ml min^{-1}). The maximum firing temperatures to avoid decomposition of the samples were determined in this way to be 865 °C for $Bi_2Al_4O_9$, 920 °C for $Bi_2Fe_4O_9$, 865 °C for $Bi_2Ga_4O_9$ and 760 °C for $Bi_2Mn_4O_{10}$.

After synthesis, the products were ground and checked for phase purity by X-ray powder diffraction (Philips PW 1700 computer-controlled diffractometer with Co Kα radiation and graphite monochromator). The Mössbauer spectrum of the ferrate was recorded using a conventional microcomputer-controlled spectrometer operating in the sinusoidal mode, using a ^{57}Co/Rh source with a maximum activity of 1.85 G Bq. The spectrum was fitted using RECOIL Mössbauer software and the isomer shifts are quoted with respect to natural iron. The ^{27}Al MAS NMR spectrum of the aluminate was acquired at 11.7 T using a Varian Unity 500 spectrometer and Doty MAS probe spun at 10–12 kHz. The spectrometer frequency was

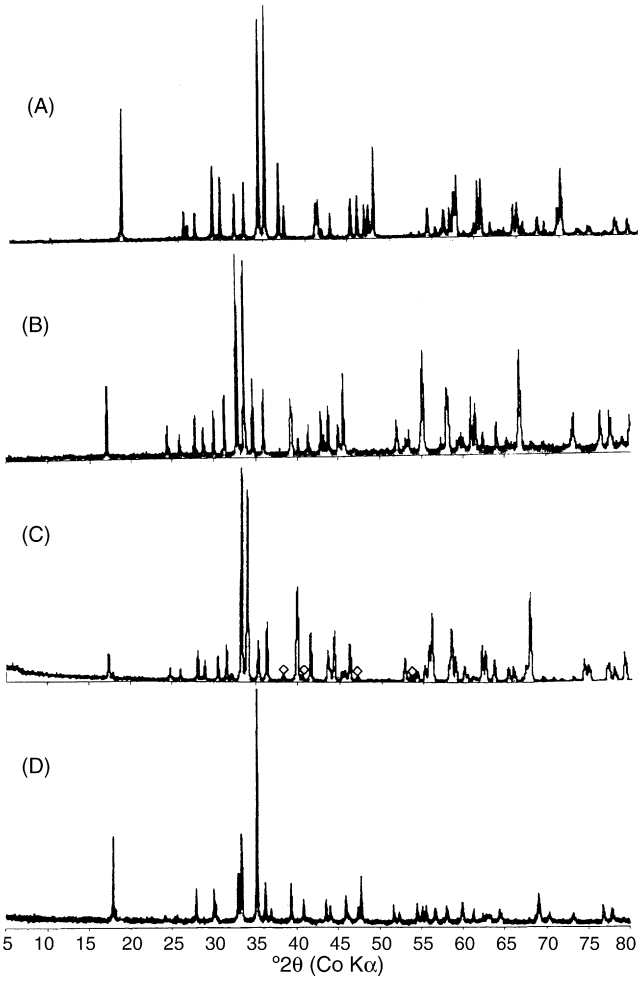

Fig. 2. XRD powder patterns of the various Bi compounds with the mullite structure synthesised in this study. (A) $Bi_2Al_4O_9$, (B) $Bi_2Fe_4O_9$, (C) $Bi_2Ga_4O_9$ (the marked peaks are from the unreacted starting material) and (D) $Bi_2Mn_4O_{10}$.

130.244 MHz and a 1 μs 15° pulse was used with a recycle delay of 1 s. The spectrum was referenced with respect to $Al(H_2O)_6^{3+}$.

The electronic measurements were made by pressing pellets 8.6 mm diameter × 0.9 mm thick at a pressure of 10 tonnes under vacuum. After sintering at the synthesis temperature, electrodes of silver paint were applied to the flat faces. The microstructure of the sintered samples was monitored by SEM (JEOL JSM-6500F with a JEPL EDS attachment).

The ac conductivity measurements were made using an Agilent 4294 A Precision Impedance Analyser. The samples were heated in a Delta 9023 IR furnace, and the polarisation versus electric field (*P–E*) hysteresis loop measurement was carried out using a modified Sawyer–Tower circuit at a frequency of 50 Hz and room-temperature.

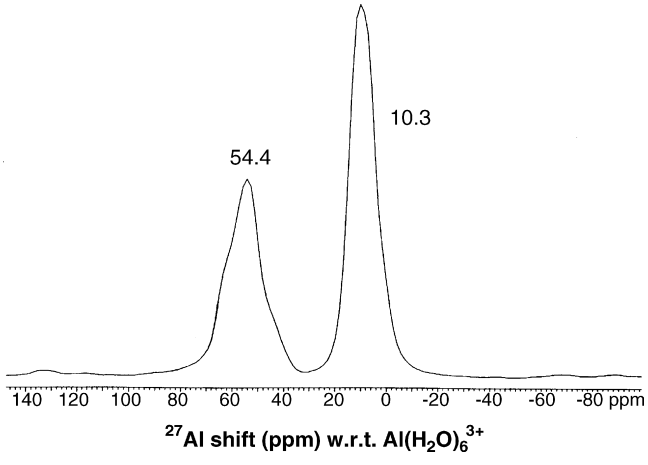

Fig. 3. 11.7 T ^{27}Al MAS NMR spectrum of $Bi_2Al_4O_9$.

3. Results and discussion

3.1. $Bi_2Al_4O_9$

The X-ray powder diffraction pattern for this compound (Fig. 2A) shows it to be monophasic, conforming to JCPDS

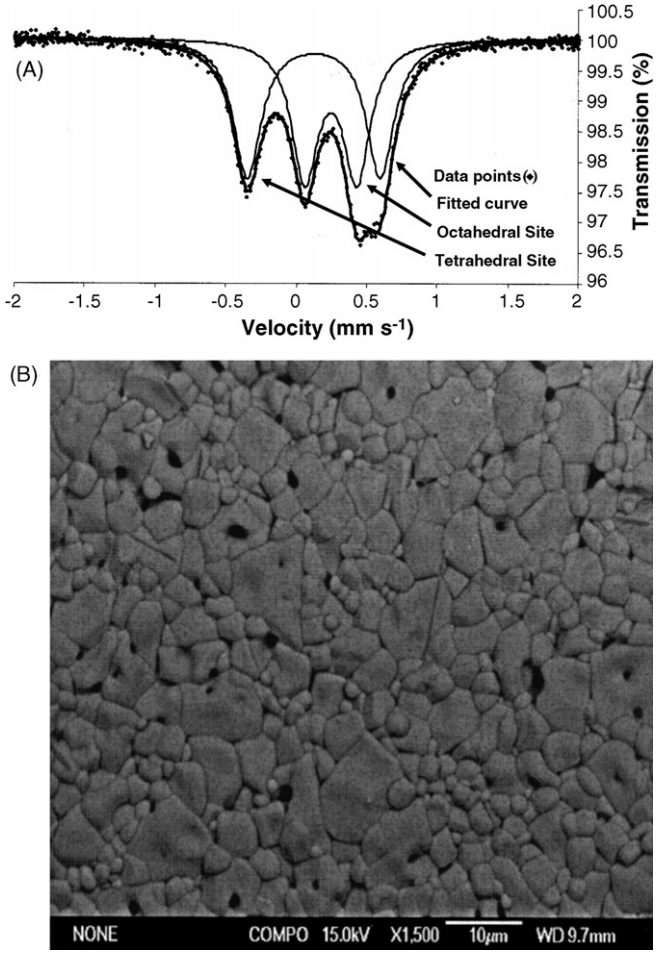

Fig. 4. (A) Room-temperature Mössbauer spectrum of $Bi_2Fe_4O_9$ and (B) back-scattered electron image of $Bi_2Fe_4O_9$ pellet sintered at 920 °C.

Table 2
Mössbauer parameters for $Bi_2Fe_4O_9$

Site	IS (mm s$^{-1)}$	QS (mm s^{-1})	Area (%)
Tetrahedral	0.1253 ± 0.382	0.9414	51.3
Octahedral	0.2462 ± 0.503	0.3690	48.7

Isomer shifts (IS) quoted with respect to natural iron.

25-1048. The ^{27}Al MAS NMR spectrum (Fig. 3) shows octahedral and tetrahedral Al resonances at 10 and 54 ppm, respectively. The asymmetric lineshape of the tetrahedral resonance is consistent with the previously reported spectrum of this compound[14] and suggests the typical quadrupolar features arising from a distorted site.

Although this compound was successfully synthesised in its pure form, it proved impossible to sinter satisfactorily at 900 °C, and at higher temperatures the sample decomposed (the decomposition temperature of 1050 °C found for the present sample is in satisfactory agreement with the literature value of 1070 °C[24]). Reaction bonding at 700 °C for 3 h followed by 12 h at 865 °C produced a sintered pellet containing an appreciable content of $12Bi_2O_3{\cdot}Al_2O_3$ which could not be removed by 5 cycles of grinding and re-firing. Accordingly, electronic measurements on this compound were abandoned.

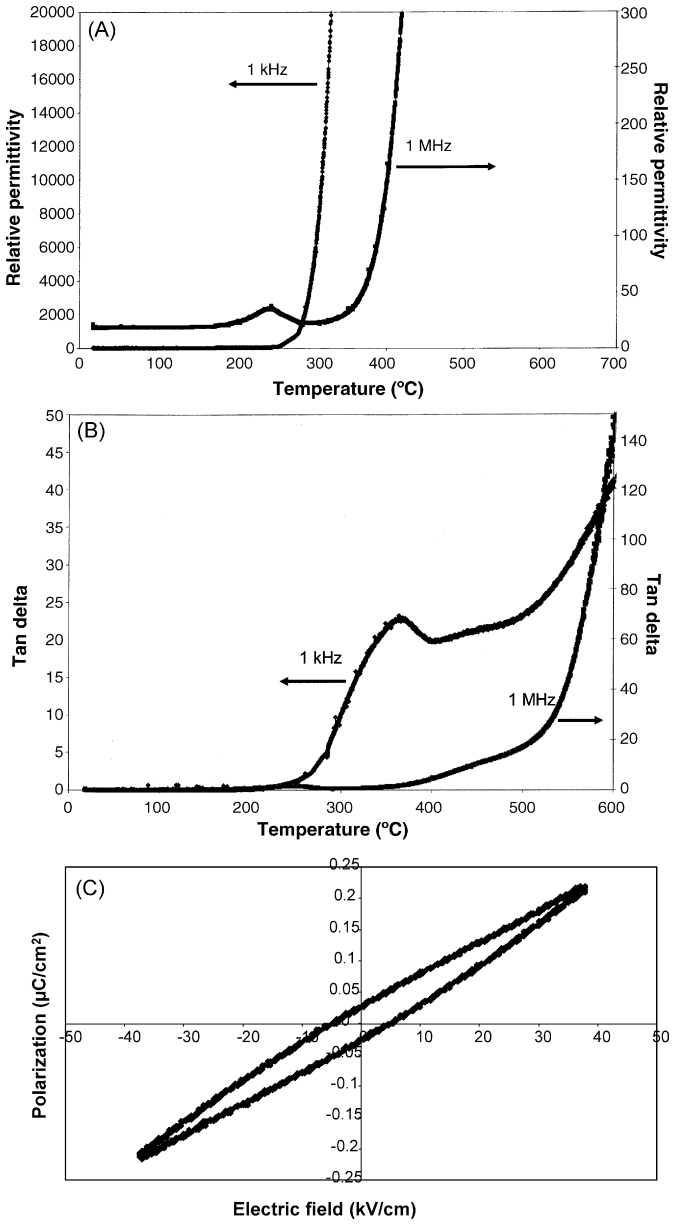

Fig. 5. Temperature dependence of (A) the relative permittivity of $Bi_2Fe_4O_9$ at high and low representative frequencies, (B) the loss angle (tan δ) of $Bi_2Fe_4O_9$ at high and low representative frequencies and (C) the room-temperature hysteresis behaviour of $Bi_2Fe_4O_9$.

3.2. $Bi_2Fe_4O_9$

The XRD pattern of this phase (Fig. 2B) shows it to be monophasic, conforming to JCPDS 25-0090. The Mössbauer spectrum of this sample (Fig. 4A) can best be fitted to two quadrupole doublets, one, with an occupancy of 48.7%, corresponding to an octahedral site and the other (51.3% occupancy) arising from the tetrahedral site. The general features of this spectrum, for which the Mössbauer parameters are shown in Table 2, are consistent with previously-reported spectra.[16,23] SEM images of the sintered pellet prior to the electronic measurements (Fig. 4B) showed a homogeneous sample with no evidence of a glassy phase.

Fig. 5A shows the temperature dependence of the relative permittivity of this sample at two representative measurement frequencies. The inflexion in the high-frequency curve, which is absent at the lower frequency, is suggestive of a transition at this temperature (252 °C), which is also reasonably close to the temperature of the reported magnetic transition in this material (264 °C[15–23]). The steep rise in permittivity at higher temperatures and all frequencies is most probably due to a steep

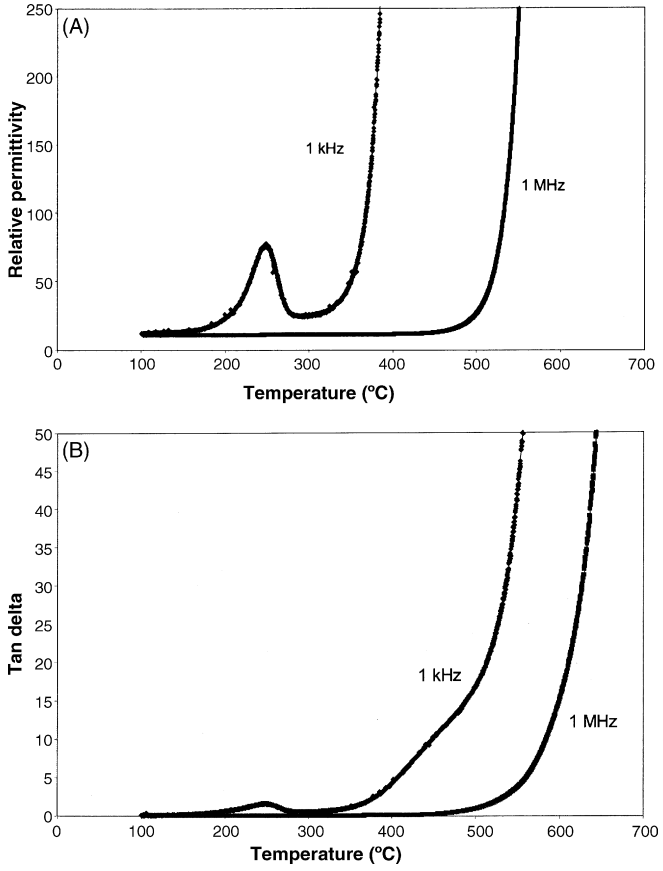

Fig. 6. Temperature dependence of (A) the relative permittivity at high and low representative frequencies and (B) the loss angle (tan δ) of $Bi_2Ga_4O_9$ at high and low representative frequencies.

increase in the dc conductivity. The temperature dependence of the loss angle (tan δ) (Fig. 5B) shows an inflexion in the low-frequency curve but not at high-frequency. This unusual behaviour may arise from dielectric relaxation in the material. The room-temperature hysteresis curve (Fig. 5C) shows very small values of the spontaneous polarization, consistent with very poor ferroelectric properties. Thus, the observed ferroelectric behaviour is as expected for a compound with a centrosymmetric crystal structure, the most noteworthy feature being a steep temperature-dependent dc conductivity.

3.3. $Bi_2Ga_4O_9$

The XRD pattern of this compound (Fig. 2C) shows it to essentially phase-pure, conforming to JCPDS file no. 37-0250, but with a trace of unreacted starting material. The relative permittivity of this phase, shown in Fig. 6A as a function of temperature, is notable for a marked inflexion at 250 °C at low frequency but not in the high-frequency curve. A similar inflexion is seen at 250 °C in the graph of the loss angle, but only at low frequency (Fig. 6B). This frequency dependence of the permittivity of $Bi_2Ga_4O_9$ is opposite to that found in the ferrate, and may be related to the presence of a trace impurity in the former, but a detailed explanation for this observation is not presently available. The frequency dependence of the loss angle is similar to that found in $Bi_2Fe_4O_9$, and as in that material, the inflexion observed at low frequency probably reflects losses due to dielectric relaxation. As with the ferrate, the steep rise in permittivity and loss angle observed at higher temperatures are due to steeply increasing dc conductivity.

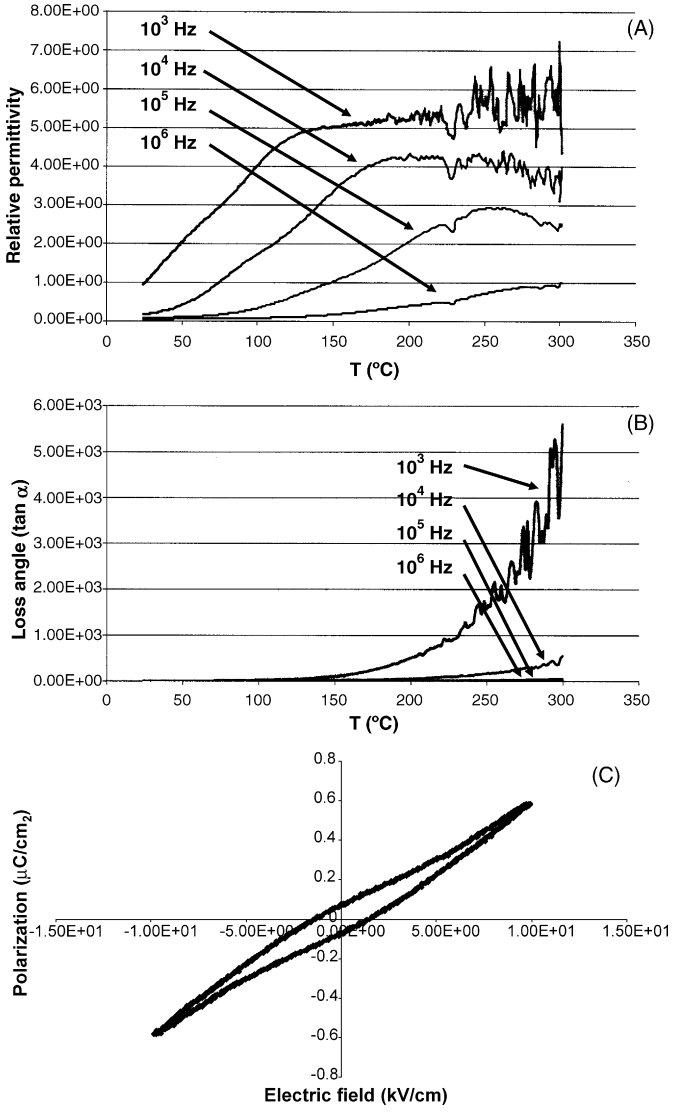

Fig. 7. Temperature dependence of (A) the relative permittivity of $Bi_2Mn_4O_{10}$ at high and low representative frequencies, (B) the loss angle (tan δ) of $Bi_2Mn_4O_{10}$ at high and low representative frequencies and (C) the room-temperature hysteresis behaviour of $Bi_2Mn_4O_{10}$.

3.4. $Bi_2Mn_4O_{10}$

The XRD pattern of this compound, synthesised and sintered at 760 °C (Fig. 2D), is consistent with JCPDS file no. 27-0048. However, the electronic measurements made on this compound were subject to considerable noise which became particularly troublesome at lower frequencies and at temperatures above about 250 °C. For this reason, the relative permittivity and loss curves for this compound (Fig. 7) are truncated at 300 °C, although the measurements were made during several cycles of heating to 900 °C. Despite the noise, the relative permittivity (Fig. 7A) may display a broad inflexion at higher frequency, similar to the behaviour of $Bi_2Fe_4O_9$, but no corresponding inflexion is seen in the loss curve (Fig. 7B), which however shows the steep rise due to increased dc conductivity with temperature common to all these compounds. The room-temperature hysteresis behaviour of the manganate (Fig. 7C) is similar to that of the ferrate, confirming that both materials are extremely poor ferroelectrics, as would be expected from their crystal structure.

4. Conclusions

All four known bismuth complex oxides with the mullite structure (the aluminate, ferrate, gallate and manganate) have been synthesised in essentially pure form by solid state reaction of the oxide. The phase-purity of the products was confirmed by X-ray diffraction and, where appropriate, ^{57}Fe Mössbauer spectroscopy and ^{27}Al MAS NMR spectroscopy. Although the synthesis and sintering temperatures were limited to at least 100 °C below the decomposition temperature, it was possible to produce mechanically strong, homogeneous pellets of all but the aluminate for electronic measurements.

The electronic properties of the pellet samples were determined as a function of frequency and temperature up to 900 °C. The relative permittivity and loss angle curves of the ferrate and gallate show frequency-dependent inflexions, some of which may be due to losses due to dielectric relaxation. However, the most notable and consistent electronic phenomenon in all samples is a steep rise in the dc conductivity at higher temperatures. The room-temperature *P–E* hysteresis curves for the ferrate and manganate are typical of very poor ferroelectric materials,

consistent with the centrosymmetric crystal structure of all these compounds.

Acknowledgements

We are indebted to K.-D. Becker and O. Bartels for obtaining the Mössbauer spectrum.

References

1. Schneider, H. and Komarneni, S., ed., *Mullite*. Wiley-VCH, Weinheim, 2005.
2. Chaudhuri, S. P., Patra, S. K. and Chakraborty, A. K., Electrical resistivity of transition metal ion doped mullite. *J. Eur. Ceram. Soc.*, 1999, **19**, 2941–2950.
3. Somiya, S. and Hirata, Y., Mullite powder technology and its applications in Japan. *Am. Ceram. Soc. Bull.*, 1991, **70**, 1624–1632.
4. Ruh, R. and Chizever, H. M., Permittivity and permeability of mullite-SiC whisker and spinel-SiC whisker composites. *J. Am. Ceram. Soc.*, 1998, **81**, 1069–1070.
5. Levin, E. M. and Roth, R. S., Polymorphism of bismuth sesquioxide. II. Effect of oxide additions on the polymorphism of B_2O_3. *J. Res. Natl. Bur. Stand., Sect. A*, 1964, **68A**, 197–206.
6. Koizumi, H. and Ikeda, T., An X-ray study on the Bi_2O_3–Fe_2O_3 system. *Japan J. Appl. Phys.*, 1964, **3**, 495–496.
7. Masuno, K., Crystal chemical studies on the Bi_2O_3–Mn_2O_3–Fe_2O_3 system. *Nipon Kagaku Zasshi*, 1967, **88**, 726–730.
8. Safronov, G. M., Speranskaya, E. I., Batog, V. N., Mitkina, G. D., Federov, P. M. and Gubina, T. F., Phase diagram of a bismuth oxide–gallium oxide system. *Zh. Neorg. Khim.*, 1971, **16**, 526–529.
9. Arpe, R. and Mueller-Buschbaum, H., Crystal structure of $Al_4Bi_2O_9$. *J. Inorg. Nucl. Chem.*, 1977, **39**, 233–235.
10. Tutov, A. G. and Markin, V. N., X-ray diffraction study of the antiferromagnetic $Bi_2Fe_4O_9$ and isotypic compounds. *Neorg. Mater.*, 1970, **6**, 2014–2017.
11. Eckerlin, P. and Liebertz, J., Preparation and crystallographic data on $Bi_2Al_4O_9$ single crystals. *Naturwiss*, 1965, **52**, 450.
12. Niizeki, N. and Wachi, M., The crystal structures of $Bi_2Mn_4O_{10}$ $Bi_2Al_4O_9$ and $Bi_2Fe_4O_9$. *Zeit. fur Kristall.*, 1968, **127**, 173–187.
13. Bloom, I., Hash, M. C., Zebrowski, J. P., Myles, K. M. and Krumpelt, M., Oxide-ion conductivity of bismuth aluminates. *Solid State Ionics*, 1992, **53–56**, 739–747.
14. Abrahams, I., Bush, A. J., Hawkes, G. E. and Nunes, T., Structure and oxide ion conductivity mechanism in $Bi_2Al_4O_9$ by combined X-ray and high-resolution neutron powder diffraction and ^{27}Al solid state NMR. *J. Solid State Chem.*, 1999, **147**, 631–636.
15. Bolkov, V. A., Kamzin, A. S. and Karapet'yan, G. Y., Determination of spin orientations in a $Bi_2Fe_4O_9$ tetrahedral sublattice by the Moessbauer effect. *Fiz. Tverd. Tela*, 1972, **14**, 2495–2498.
16. Kostiner, E. and Shoemaker, G. L., Mossbauer effect study of $Bi_2Fe_4O_9$. *J. Solid State Chem.*, 1971, **3**, 186–189.
17. Petrakovskii, G. A., Sablina, K. A., Volkov, V. E., Stolovistskii, I. M., Chechernikov, V. I. and Yakovenko, V. L., Magnetic resonance and optical properties of the amorphous magnetic substrate bismuth ferrite ($Bi_2Fe_4O_9$). *Zh. Eksper. Teor. Fiz.*, 1983, **85**, 592–601.
18. Sablina, K. A., Federov, Y. M., Volkov, V. E. and Korets, A. Y., Optical and magnetic studies of bismuth iron oxide ($Bi_2Fe_4O_9$) glass. *Magn. Elektr. Rezon. Svois. Magnit.*, 1982, 126–131.
19. Sablina, K. A., Piskorskii, V. P. and Agartanova, E. N., Effect of amorphization on the magnetic properties of antiferromagnetic bismuth iron oxide ($Bi_2Fe_4O_9$). *Rezon. Magnit. Svois. Magnit.*, 1978, 110–115.
20. Shamir, N., Gurewitz, E. and Shaked, H., The magnetic structure of bismuth ferrite ($Bi_2Fe_4O_9$)—a neutron diffraction study. *J. Magn. Magn. Mater.*, 1978, **7**, 66–68.
21. Shamir, N., Gurewitz, E. and Shaked, H., The magnetic structure of bismuth ferrite ($Bi_2Fe_4O_9$)—analysis of neutron diffraction measurements. *Acta Cryst. A*, 1978, **A34**, 662–666.
22. Sitter, J. D., Dauwe, C., Grave, E. D., Govaert, A. and Robbrecht, G., On the magnetic properties of the basic compounds in the Bi_2O_3–Fe_2O_3 system. *Physica*, 1977, **86–88**, 919–920.
23. Bokov, V. A., Novikov, G. V. and Trukhtanov, V. A., Iron-57 Moessbauer effect in $Bi_2Fe_4O_9$. *Fiz. Tverd. Tela*, 1969, **11**, 2871–2873.
24. Speranskaya, E. I., Skorikov, V. M., Safronov, G. M. and Gaidukov, E. N., Bismuth oxide–aluminium oxide system. *Neorg. Mater.*, 1970, **6**, 1364–1365.